Advance prediction of coastal groundwater levels with temporal convolutional and long short-term memory networks

Xiaoying Zhang[a,b], Fan Dong[a,b], Guangquan Chen[c], Zhenxue Dai[a,b]*

[a] Institute of Intelligent Simulation and Early Warning for Subsurface Environment, Jilin University, Changchun, China

[b] College of Construction Engineering, Jilin University, Changchun , China

[c] Key Laboratory of Marine Sedimentology and Environmental Geology, First Institute of Oceanography, State Oceanic Administration, Qingdao, China

* Correspondence: Zhenxue Dai, dzx@jlu.edu.cn

Highlights

- TCN- and LSTM-based models were proposed to predict groundwater levels in a coastal aquifers

- Tidal, precipitation and groundwater levels were utilized as input data in the networks

- In advance 1- day, 3-, 7- and 15-days groundwater levels were predicted with the highest accuracy of 1-day-lead prediction

- The TCN-based model slightly outperformed the LSTM-based model in accuracy but less efficiency

Abstract

Prediction of groundwater level is of immense importance and challenges for the coastal aquifer management with rapidly increasing climatic change. With the development of artificial intelligence, the data driven models have been widely adopted in hydrological processes management. However, due to the limitation of network framework and construction, they are mostly adopted to produce only one-time step in advance. Here, the temporal convolutional network (TCN) and long short-term memory

(LSTM) based models were developed to predict groundwater levels with different leading periods in a coastal aquifer. The beginning hourly-monitored ten-month data in two monitoring wells were used for model training and testing, and the data of the following three months were used as prediction with 24, 72, 180 and 360 time steps (1-day, 3-, 7- and 15-days) in advance. The historical precipitation and tidal level data were incorporated as input data. For one-step prediction of the two wells, the calculated R^2 of the TCN-based models values were higher and the RMSE values were lower than that of the LSTM-based model in the prediction stage with shorter running times. For the advanced prediction, the model accuracy decreased with the increase of advancing period from 1-day to 3-, 7- and 15-days. By comparing the simulation accuracy and efficiency, the TCN-based model slightly outperformed the LSTM-based model but less efficient in training time. Both models showed great ability to learn complex patterns in advance using historical data with different leading periods, and had been proved to be valid localized groundwater level prediction tools in the subsurface environment.

Keywords: prediction; Groundwater level; Coastal aquifer; Temporal convolutional networks; Long Short-Term Memory

1 Introduction

As the economic development and population escalate in coastal area, the fresh

groundwater needs continue to mount, seawater intrusion has post great threat to the availability of portable water resources globally (Baena-Ruiz et al., 2018). In United States, Mexico, Canada, Australia, China, India, South Korea, Italy and Greece with dense population, many coastal aquifers have experienced salinization caused by seawater intrusion (Barlow and Reichard, 2009; Park et al., 2011; Pratheepa et al., 2015; Zhang et al., 2017; Lu et al., 2013). Protection projects such as aquifer replenishment can be constructed to alleviate seawater intrusion by artificially increasing groundwater recharge in the aquifer than what occurs naturally (Abdalla and Al-Rawahi, 2012; Lu et al., 2019). The replenishment programs have been operated in developed area such as Perth, Western Australia, and California, USA (Garza-Díaz et al., 2019). The infrastructures tend to be costly and out of reach for many developing countries. A reliable seawater intrusion monitoring and predicting system is still essential and is recognized as the most effective way of keeping freshwater water from contamination of seawater (Xu and Hu, 2017).

In the past several decades, conventional numerical models have been widely utilized to simulate and predict the groundwater fluctuation dynamics and chemical variations (Batelaan et al., 2003; Dai et al., 2020; Huang et al., 2015; Li et al., 2002). However, the difficulty of acquiring extensive hydrological and geological data and setting reasonable boundaries limits its application on seawater intrusion management. Meanwhile, the method is not suitable to simultaneously adopt updated monitoring data and produce real-time prediction. Under such circumstances, where data source is scarce, artificial intelligence technology has been proposed in groundwater dynamic

prediction. Artificial neutral network (ANN) has been greatly improved and became a robust tool for dealing groundwater problems, where the flow is nonlinear and highly dynamic in nature (Maier and Dandy, 2000). The conventional network model generally has defects such as high computational complexity, slow training speed, and failure in retaining historical information, thus is hardly to be enrolled in the long-term time-series prediction (Cannas et al., 2006; Mei et al., 2017). To solve this problem, researchers upgraded the conventional networks by integrating them with methods like genetic algorithm (Danandeh Mehr and Nourani, 2017; Ketabchi and Ataie-Ashtiani, 2015), singular spectrum (Sahoo et al., 2017), and wavelet transform (Gorgij et al., 2017; Seo et al., 2015; Zhang et al., 2019). Singular spectrum analysis and wavelet transform can help to preprocess the time-series data before they are put into the neural networks to improve prediction accuracy and efficiency.

With the computing capacity development, deep learning (DL) has emerged as a very powerful time-series prediction method. DL models are particularly suitable for big data time-series, because they can automatically extract complex patterns without feature extraction preprocessing steps (Torres et al., 2019). However, the general fully connected networks are not effective to capture the temporal dependence of time-series (Senthil Kumar et al., 2005). Therefore, more specialized DL models, such as recurrent neural networks (RNN) (Rumelhart et al., 1986) and convolutional neural networks (CNN) (Lecun et al., 1998) have been adopted in the field of time-series prediction (Feng et al., 2020). Different from the back-propagation (BP) neural network that the information flows from the input to the output layer in one direction, the RNN preserves

94 the information from the previous step as input to the current step with loops (Coulibaly

95 et al., 2001). This allows the RNN to handle time-series and other sequential data but

96 generally is not straightforward for a long-term calculation in practice (Bengio et al.,

97 1994). Therefore, the enhanced RNN model, long short-term memory (LSTM) is

98 proposed and capable to process high variable-length sequences even with millions of

99 data points (Fischer and Krauss, 2018; Kratzert et al., 2019) . As one of the best deep

100 neural network model in time-series predicting, the LSTM has been widely used in the

101 prediction of temporal variations such as stock market predictions (Fischer and Krauss,

102 2018), rainfall-runoff (Kumar Dubey et al., 2021) and groundwater level (Solgi et al.,

103 2021). Despite of substantial progresses in hydrology predicting, these networks still

104 have issues of low training efficiency and low accuracy (Zhan et al., 2022).

105   More recently, a variant of the CNN architecture known as temporal convolutional

106 networks (TCN) has acquired popularity (Bai et al., 2018). The prominent characteristic

107 of TCN is its ability to capture long-term dependencies without information loss (Cao

108 et al., 2021). Meanwhile, it joints a residual block structure to fix the disappearance of

109 gradient in the deep network structure (Chen et al., 2020). With proper modifications,

110 the TCN is quite genetic and easily to be used to build a very deep and extensive

111 network in sequence modeling. In earth science, the TCN has been successfully applied

112 to time-series prediction tasks including multivariate time-series predicting for

113 meteorological data (Wan et al., 2019), probabilistic predicting (Chen et al., 2020) and

114 wind speed predicting (Gan et al., 2021). Researches suggest that the TCN convincingly

115 has advantage in ~~several~~ popular deep learning models across a broad range of sequence

116 modeling tasks (Borovykh et al., 2019; Chen et al., 2020; Wan et al., 2019). Another

117 import subject is that these networks are mostly used to predict variables in only one

118 step, which is not enough for the prediction of hydrology information in management.

119 Researches have been adopted the method to predict the trends of ENSO and sea

120 temperature (Yan et al.,2020; Jian et al., 2021). However, the potential of TCN has not

121 been investigated in the sequencing model of hydrogeology field. Therefore, it is

122 worthy to explore their prediction abilities in leading periods.

123   The objective of this study is to develop real-time advance prediction climate-

124 dydro hybrid data-driven models of groundwater level in the coastal aquifer based on

125 TCN and LSTM. The hourly processed tidal, precipitation with groundwater level data

126 in monitoring wells of Laizhou Bay are utilized to train model and prediction the

127 groundwater level in a period of 1-day, 3-,7- and 15-days. The two models were further

128 compared in the view of accuracy and efficiency. The rest of the paper is organized as

129 follows. Sect. 2 introduces the study area and observational data. Sect. 3 illustrates the

130 detailed concepts of TCN and LSTM, the experimental model settings and model

131 evaluation criteria. Sect. 4 presents the predicting results and discussions. Finally, the

132 paper is concluded in Sect. 5.

133 **2 Study area and data processing**

134 **2.1 Site description**

135   The study area is located in the south coast of Laizhou Bay, along the Yangzi to

136 Weifang section in Shandong province of China (Fig. 1). The Laizhou Bay is one of the

137 earliest and most seriously affected area by seawater intrusion since 1970s in China

138 (Han et al., 2014; Zeng et al., 2016). The area is ~~basically~~ a coastal plain, which contains

139 a series of Cretaceous to modern sediments that covering the Paleozoic basement. The

140 sedimentary facies of coastal aquifer are alluvium, proluvial and marine sediments from

141 south to north (Han et al., 2011). According to the research of (Xue et al., 2000), there

142 ~~have been~~were three seawater intrusion and regression events in the sea area of Laizhou

143 Bay since the upper Pleistocene. The transgression in the early upper Pleistocene

144 formed the third marine aquifer containing sedimentary water. These brine were formed

145 by evaporation and concentration of ancient seawater and re-dissolution and mixing of

146 salt (Dai and Samper, 2006; Zhang et al., 2017). The monitoring wells BH01-BH05 are

147 distributed in the study area along a cross section perpendicular to the coastline. Among

148 the wells, the ~~data of~~ well BH01 and BH05 ~~are~~have relatively integrate data in time and

149 distributed in the two sides of the cross profile with distinguished annual variation

150 pattern, which are selected as examples for the developed models.

151

152  Figure 1. Schematic figure of the study area with monitoring wells BH01-BH05.

2.2 Data collection and pre-processing

154  The precipitation and tidal level are selected as the primary factors to affect the

155 groundwater dynamics in the coastal area. The data in the period of 2011 to 2012 with

156 groundwater level observations of ~~three~~wo wells are combined as the input of the deep

157 learning models. A total of ~~37~~28,~~920~~836 data items are collected for monitoring wells

158 and the variations of groundwater level, and tidal level with precipitation are shown in

159 Figure 2. The rainfall is concentrated from June to September and in shortage from

160 December to April. The tide in the study area is irregular mixed with a semi-diurnal

161 variation. In the experiments, ten months of data from October 2011 to July 201~~1~~2 is

162 first extracted for model training and testing. The rest of the data from August 2012 to

163 October 2012 is used to test model prediction accuracy.

164  In addition, the magnitudes of meteorological and hydrological variables have

165 obvious temporal variations. To reduce the negative impact on the model learning

166 ability, especially on the speed of gradient descent, all variables are normalized to

167 ensure that they remain at the same scale (Kratzert et al., 2019). This pre-processing

168 method ensures the stable convergence of parameters in the developed TCN- and

169 LSTM-based models and improve the simulation accuracy of the model. The

170 normalization formula is as follows:

$$x'_i\cancel{y}_i = \frac{x_i - x_{min}}{x_{max} - x_{min}} \tag{1}$$

172 where x_i represents the original data in time i; and x_i represents the original data in time

173 i x_{max} and x_{min} are the maximum and minimum variable values. The output of the

174   network is retransformed to obtain the final groundwater level prediction, which is an

175   inverse data scaling process.
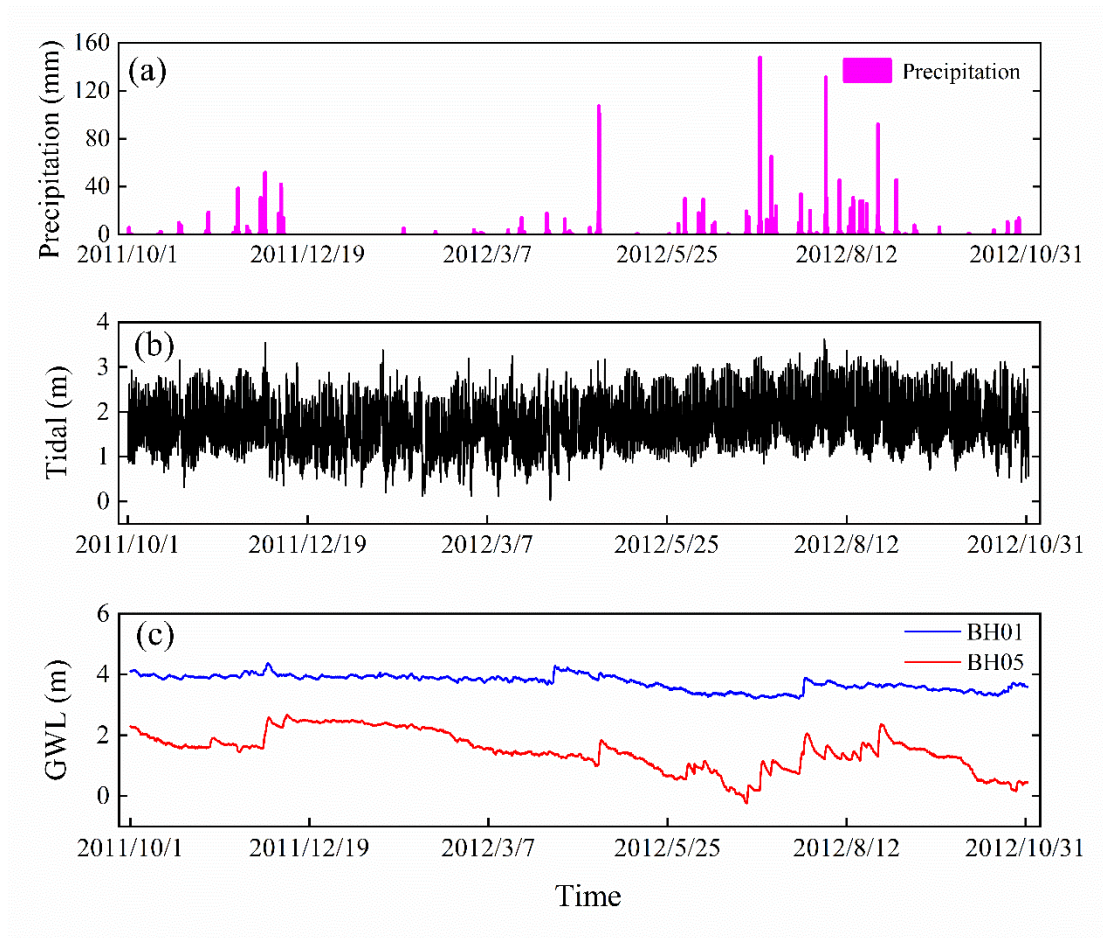
176

177   Figure 2. Time-series of the variables in the study, including (a) precipitation, (b) tide,

178   (c) groundwater level (GWL).

3 Methodology

3.1 Temporal Convolutional Network

181   The TCN is first proposed for video action segmentation and detection by

182   hierarchically capturing intermediate feature presentations. Then the term is extended

183   for sequential data for a wide family of architectures with generic convolution (Bai et

184   al., 2018; Lea et al., 2017). Suppose that we have an input hydro-climate sequence at

185   different times x_0, ..., x_T, the goal of the modeling is to predict the corresponding

186 groundwater level as outputs y_0, ..., y_T at each time. The problem could transfer to build

187 a network f that minimizes the function loss between observations and actual network

188 outputs $L[(y_0, ..., y_T,),(\hat{y}_0,...,\hat{y}_T)]$, where $\hat{y}_0,...,\hat{y}_T = f(x_0, ..., x_T)$. Currently, a typical

189 TCN consists of dilated, causal 1D full-convolutional layers with the same input and

190 output lengths. With TCN, the prediction y_t depends only on the data from x_0 and x_t and

191 not include the future data from x_t and x_T (Yan et al., 2020). With the three key

192 components of TCN, it has two distinguishing characteristics: (1) the TCN is able to

193 map the same length of output as the input sequence as in RNN; (2) the convolution

194 involved in TCN is causal, eliminating the influence of future information on the output.

195 3.1.1 Causal Dilated Convolutions

196   In the TCN, the first advantage is accomplished by a 1D full-convolutional network

197 (FCN) architecture. Different from the traditional CNN, the FCN transforms the fully

198 connected layers into the convolutional layers for the last layers, preserving the same

199 length of output as that of the input (Long et al., 2015). As shown in Fig. 3a, the lengths

200 of the input, the hidden and the output layers are the same in the FCN. Some zero

201 padding is needed in this step by adding additional zero-valued entries with a length of

202 kernel size-1 in each layer. The kernel size is the number of successive elements that

203 are used to produce one element in the next layer.

204   To avoid the information leakage from the future (after time t), the TCN uses

205 causal convolution instead of standard convolution, where only the elements at or

206 before time t in the previous layer are adopted into the mapping of the output at time t.

207 Further, the dilated convolution is employed to capture long-term historical information

208   by skipping a given step size (dilation factor *d*) in each layer. For example, the dilation

209   factor *d* increases from 1 to 4 with the evolution of the network depth (*n*) in an

210   exponential increasing pattern. In this way, a very large receiving domain is created and

211   all the historical records in the input can be involved in the prediction model with a

212   deep network.

213
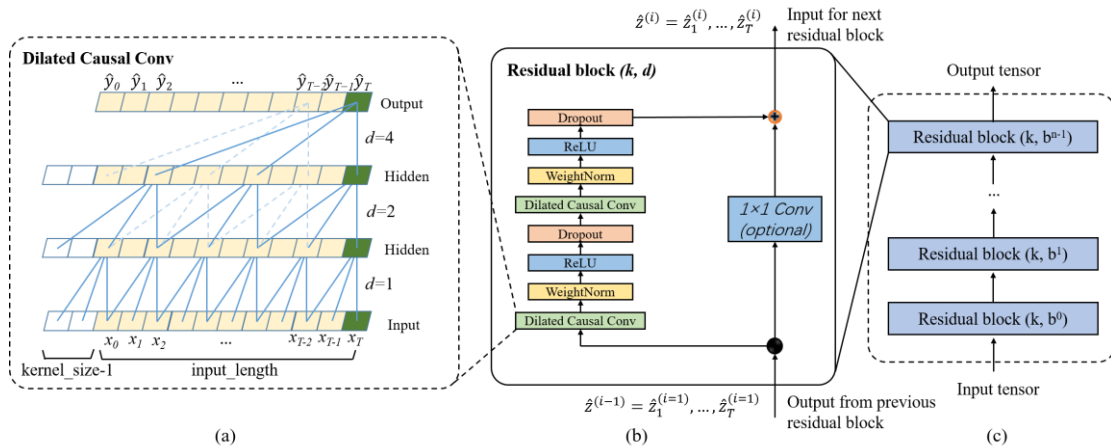
214   Figure 3. Architectural elements in the proposed TCN. (a) the structure of causal dilated

215   convolution; (b) the TCN residual block. An 1x1 convolution is added when residual

216   input and output have different dimensions; (c) framework of residual connection in the

217   TCN.

218   3.2.2 Residual Connections

219   In a high dimensional and long-term sequence, the network structure could be very

220   deep with increasing complicity and cause a vanishing gradient. To solve this issue, a

221   residual block structure is introduced to replace the simple 1D causal convolution layer,

222   so that the designed TCN structure is more generic (He et al., 2016). The residual block

223   in a TCN is represented in Fig. 3b. It has two convolutional layers with the same kernel

224   size and dilation factor and non-linearity. To solve non-linear models, the rectified

225 linear unit (ReLU) is added to the top of the convolutional layer (Nair and Hinton, 2010).

226 The weight normalization is applied between the input of hidden layers (Salimans and

227 Kingma, 2016). Meanwhile, a dropout is added after each dilated convolution for

228 regularization (Srivastava et al., 2014). For all connected inner residual blocks, the

229 channel widths of input and output are consistent. But the width may be different

230 between the input of the first convolutional layer of the first residual block and the

231 output of the second convolutional layer of the last residual block. Therefore, a 1×1

232 convolution is added in the first and last residual block to adjust the dimensions of the

233 residual tensor into the same. The output of the residual block is represented by $\hat{Z}^{(i)}$ for

234 the ith block.

235 3.2.3 Structure of TCN

236  A complete structure of TCN is illustrated in Fig.3c. It contains a series of

237 proceeding residual blocks. The structural characteristics make TCN a deep learning

238 network model very suitable for complex time-series prediction problems (Lara-

239 Benítez et al., 2020). The main advantage of TCN is that, similar to RNN, they have

240 flexible receptive fields and can deal with various length input by sliding one-

241 dimensional causal convolution kernel. Furthermore, because TCN shares a

242 convolution kernel and has parallelism, it can process long sequences in parallel instead

243 of sequential processing like RNN, so it has lower memory usage and shorter

244 computing time than a cyclic network. Moreover, RNN often has the problems of

245 gradient disappearance and gradient explosion, which are mainly caused by sharing

246 parameters in different periods, while TCN uses a standard backpropagation-through-

247 time algorithm (BPTT) for training, so there is little gradient disappearance and

248 explosion problem (Pascanu et al., 2012). The detailed mathematical calculation and

249 associated information of the TCN architecture are referred to (Bai et al., 2018).

3.2 Long Short-Term Memory network

251 LSTM is a special RNN model explicitly designed for long-term dependence

252 problems. As shown in Fig. 4a, the RNN has a series of repeating modules that

253 recursively connected in the evolution direction of the sequence. The chain-like

254 structure permits the RNN to retain important information in a "tanh" layer and produce

255 the same length of output $\hat{y}_t$ as input x_t. However, the short-length "remember time" is

256 not enough for the groundwater prediction. Especially for our hourly recorded data, a

257 maximum step about ten reported by Bengio et al. (1994) is unable to count the effect

258 of annually, seasonally, and even daily groundwater variation. Different from the simple

259 layer in the RNN, the LSTM has a more complicated repeating module with four

260 interacting layers.

261 The core idea of LSTM is the special structure to control the cell state in the

262 module as shown in Fig. 4b. It includes a cell and an input gate i_t, a forget gate f_t, and

263 an output gate o_t. The information can directly flow down along cells C without critical

264 changes, therefore, preserving long-term history messages (Zhang et al., 2018b). The

265 three gates control which data in a sequence is important to keep or throw away, and

266 protect the relevant information passed down in the cell to make predictions. The forget

267 gate f_t has a sigmoid layer to determine which information is discarded with a value

268 between 0 and 1. The lower the value, the less the information added to the cell state

269   (Ergen and Kozat, 2018). Opposite the forget gate, the input gate i_t decides what

270   information to retain in the cell state. It is composed of two parts: a sigmoid layer and

271   a tanh layer. The two layers are combined to govern which values will be updated by

272   generating a new candidate value $\tilde{C}_t$. The old cell state C_{t-1} then can be updated into

273   the new cell state C_t with a weighted function. Finally, the output gate o_t determines

274   what parts of the cell state should be passed on to the next hidden state. The detailed

275   calculation of the LTSM can be referenced to (Lea et al., 2016).

276

277
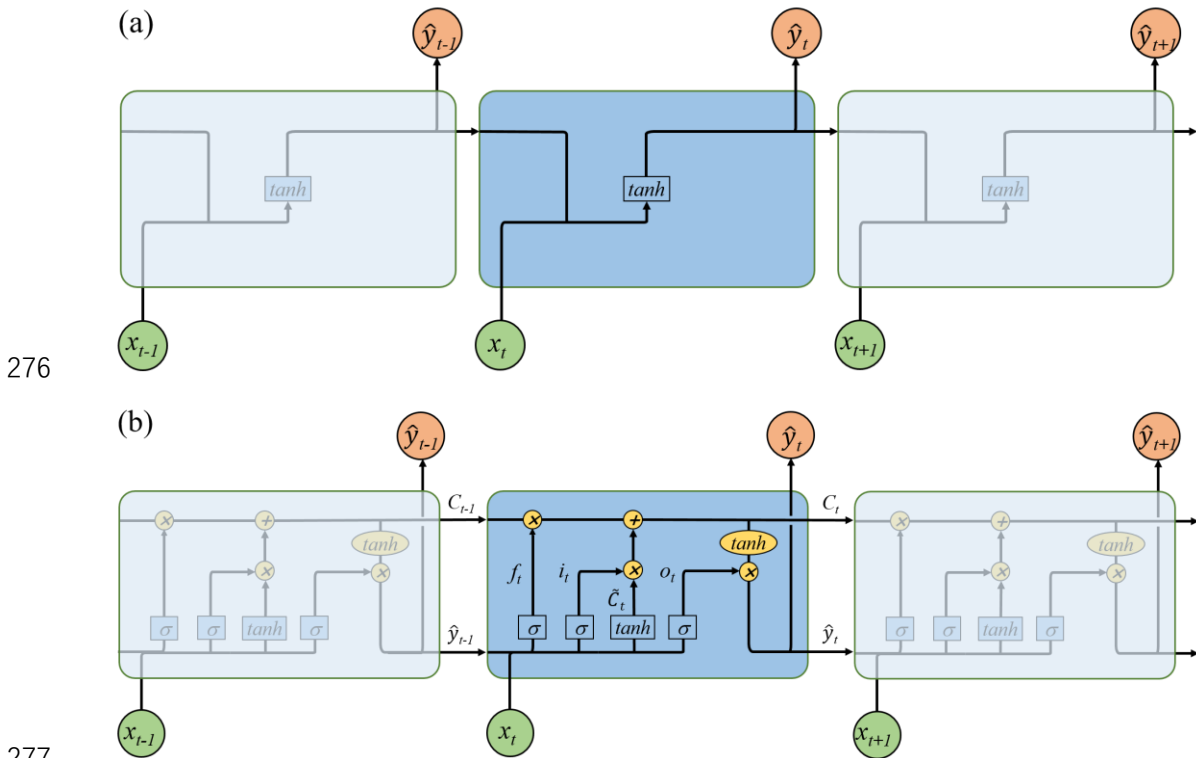
278   Figure 4. Graphical representation for (a) chain like structure of the RNN by assigning

279   x_t and $\hat{y}_t$ as input and output. The self-connected hidden units allow information to be

280   passed from one step to the next; (b) LSTM's memory block based on RNN. The

281   hidden block includes three gates (input i_t, forget f_t, output o_t) and a cell state to select

282   and pass the historical information.

3.3 Experimental study

The TCN- and LSTM-based models were developed separately for monitoring wells BH01 and BH05. Due to the high complexity of the DL models, setting appropriate hyper-parameters for the developed networks is very important. Here, the impact of the size of the input window, the epoch number and the batch size were tested with different convolutional architectures over the monitoring data (Lara-Benítez et al., 2020). The learning dataset is first divided into two parts: 80% of the time-series data is used as training set, and 20% of the data is utilized as testing set. The effect of different splitting strategies is further tested in section 4. With the increase of the epoch numbers, the curve gradually approaches to the optimal fitting state from the initial non-fitting state, but too many epochs frequently lead to over-fitting of the neural network (Afaq and Rao, 2020). Meanwhile, the number of iterations generally increases for updating weights in the neural network. Therefore, the number of epoch from 0 to 300 is evaluated. Batch size represents the number of samples between model weight updates (Kreyenberg et al., 2019). The value of the batch size often is set between 1 and hundreds. Larger batch size often leads to faster convergence of the model, but may lead to less ideal of the final weight set. To find the best balance between memory efficiency and capacity, the batch size should be carefully set to optimize the performance of the network model. Besides these parameters, the number of filters in the TCN-based and the hidden nodes in the LSTM-based model were as well tested within reasonable ranges.

The 1-day, 3-, 7-, and 15-days leading prediction experiments were further

conducted to test the capacity of DL methods in predicting long-term groundwater level

in the coastal aquifer. To eliminate the randomness of model training, all experiments

were repeated 5 times and the average values of each index were compared. In all

experiments, the average absolute error (MAE) has been used as the loss function of

networks (Lara-Benítez et al., 2020). The Adam optimizer has an adaptive learning rate,

which can improve the convergence speed of deep networks, which has been used to

train the models (Kingma and Ba, 2015).

3.4 Evaluation of model performance

Two evaluation metrics, coefficient of determination (R^2) and root mean square

error (RMSE) are selected to quantify the goodness-of-fit between model outputs and

observations (Zhang et al., 2020). The two criteria are calculated using the following

equations:

$$RMSE = \sqrt{\frac{1}{N}\sum_{i=1}^{N}(h_i - y_i)^2} \tag{1}$$

$$R^2 = \frac{\sum_{i=1}^{N}(h_i - \bar{h})^2 - \sum_{i=1}^{N}(h_i - y_i)^2}{\sum_{i=1}^{N}(h_i - \bar{h})^2} \tag{2}$$

where h_i is the observed groundwater level at time i, y_i is the network prediction values

at time i, $\bar{h}$ is mean of the observed groundwater levels, and n is the number of

observations. RMSE measures the prediction precision which creates a positive value

by squaring the errors. The RMSE score is between [0, ∞]. If the RMSE approaches to

0, the model prediction is ideal. R^2 measures the degree of model replication results,

ranging between [−∞, 1]. For the optimal model prediction, the score of R^2 is close to

1.

4 Results and discussions

4.1 Hyper-parameter trial experiments

4.2.1 Experiments of the TCN-based model

The TCN-based model was built on Keras platform using TensorFlow of python as the backend. Taken the groundwater level prediction data set in well BH01 as an example, the trials were set up with a variety combination of different hyper-parameters in the TCN-based model as illustrated in Table 1. With the fixed number of epoch, the simulation results of 32 filters were better than that of 16 and 64 filters. Meanwhile, under the condition of 32 filters, the accuracy of the model decreased with the increasing of batch size. The results of the 16 batch size were better than that of 32 and 64 batches. Based on the above experimental results, the influence of different numbers of epoch on the simulation was further explored with the filters was 32 and the batch size was 16 as shown in Fig.5. The overall results of the model were improved when the number of epoch increased from 100 to 190 though the variation was not strictly linear, and the variations became stable with minor fluctuations when the number of epoch exceeded 200.

Table 1. The RMSE and R^2 values between the observed and predicted groundwater levels in well BH01 with different numbers of epochs, different numbers of filters, and different batch sizes. The bold values represent the optimal hyper-parameters with the smallest RMSE and the highest R^2 scores in the TCN-based model.

Epoch	Filters	Batch size	RMSE(m)	R^2	Time(min)
		16	0.0182	0.9904	1.29

100	32	32	0.0117	0.9876	1.05
		64	0.0117	0.9875	0.78
200	16	16	0.0078	0.9946	2.41
		32	0.0068	0.9959	1.75
		64	0.0090	0.9942	1.19
200	**32**	**16**	**0.0059**	**0.9970**	2.58
		32	0.0075	0.9948	2.01
		64	0.0082	0.9938	1.51
200	64	16	0.0125	0.9906	3.68
		32	0.0101	0.9907	3.21
		64	0.0157	0.9775	2.76
300	32	16	0.0065	0.9955	3.8
		32	0.0076	0.9946	3.01
		64	0.0099	0.9904	2.22

347
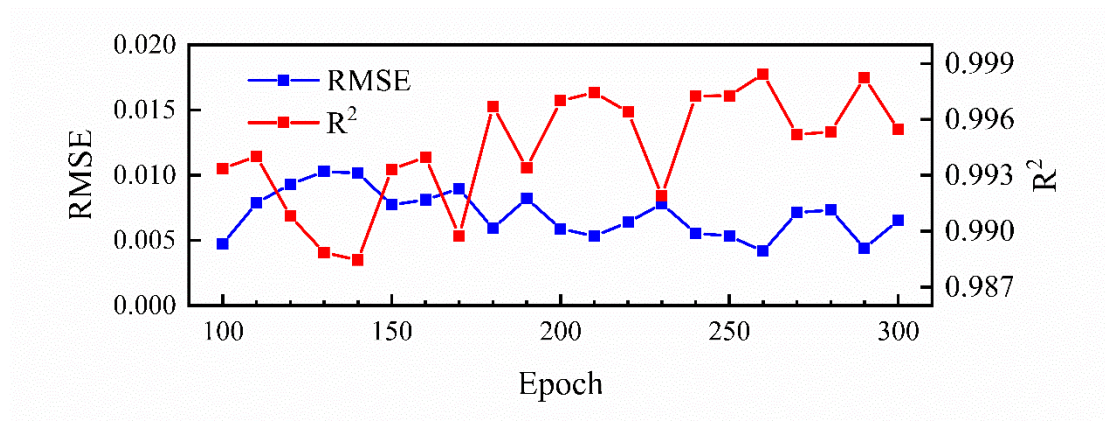
348

349 Figure 5. The variation of RMSE and R^2 values between the observed and predicted

350 groundwater levels of well BH01 with the increasing number of epoch when the number

351 of filters is 32 and the batch size is 16.

4.2.2 Experiments of the LSTM-based model

353   The number of epochs and hidden nodes are two key parameters affecting the

354 simulation accuracy of LSTMs (Zhang et al., 2018a). Different hyper-parameter

355 combinations were tested as well as in the proposed TCN-based model with

356 groundwater levels in well BH01. The RMSE, R^2 and running time are shown in Table

357 2. With a fixed number of hidden nodes, the results of 100 and 200 epochs were better

358 than that in the 300 epochs experiment. A detailed variation of RMSE and R^2 values

359 with increasing number of hidden nodes and epochs is further illustrated in Fig. 6. The

360 figure shows that the RMSE and R^2 have a decreasing and increasing trend separately

361 when the number of epochs is greater than 150, but is reversed when it is larger than

362 240. The variations of RMSE and R^2 with increasing hidden nodes have similar changes

363 as shown in Table 2. Though an insufficient number of neurons may decrease the

364 learning ability of the network, the results indicate that an increasing training hyper-

365 parameters may not necessary to ensure better prediction.

366 Table 2. The RMSE and R^2 values between the observed and predicted groundwater

367 levels in well BH01 with different numbers of epochs and hidden nodes. The bold

368 values represent the optimal hyper-parameters used in the proposed LSTM-based

369 model.

Epoch	Hidden nodes	RMSE	R^2	Time(min)
100	50	0.0104	0.9902	1.01
	60	0.0098	0.9916	1.38
	70	0.0095	0.9922	1.53
	80	0.01	0.9913	1.75
200	50	0.0094	0.9922	1.91
	60	0.0089	0.9931	2.59
	70	**0.0088**	**0.9932**	**2.96**
	80	0.0092	0.9925	3.28
300	50	0.0101	0.9903	2.86
	60	0.0105	0.9901	3.85

70	0.0103	0.9907	4.29
80	0.0120	0.9872	4.92
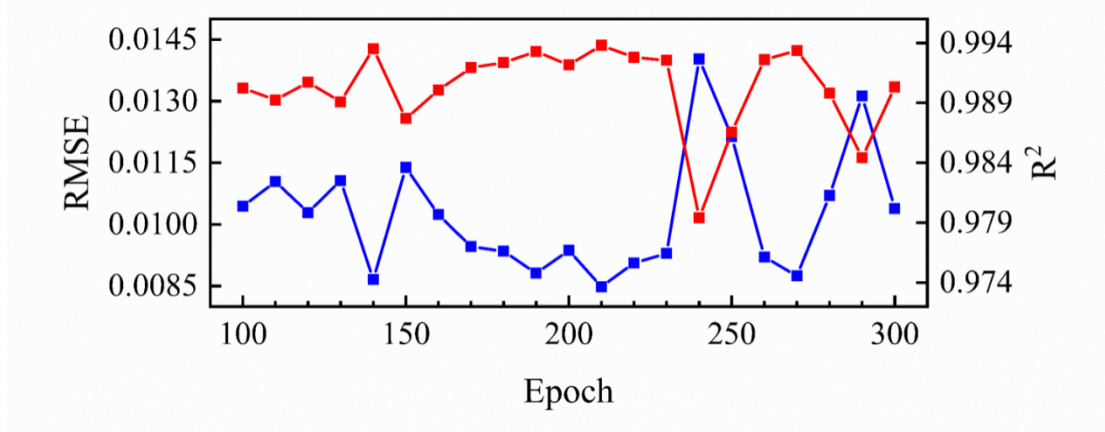
Figure 6. The variation of RMSE and R^2 values between the observed and predicted groundwater levels of well BH01 with the increasing of the number of epochs when the hidden node is 50.

The trial experimental results present similar fitting pattern shared by the two kind of networks. The growing value of parameters dramatically increases the computational cost in the network. For example, the time cost from 50 to 80 hidden nodes has increased about 1.7 times in each iteration trial in the LSTM-based model. Finally, 200 epochs, 32 filters, and the 16 batch size were chosen as the optimal parameters in the TCN network. For the LSTM network, the number of epoch and hidden nodes were chosen as 200 and 70.

4.3 Model performance and evaluation

The optimal hyper-parameters of the proposed TCN-based model for groundwater level predicting are shown in Table 1 (epoch = 200, filters = 32 and batch size = 16). Besides that, the kernel size in each convolutional layer is set as 6, the

386 dilations are [1,2,4,8]. For the LSTM-based model, the batch size is set to 148 with

387 epoch=200 and nodes=70. The same hyper-parameters are then utilized to construct

388 TCN and LSTM architectures for prediction of groundwater level in different

389 monitoring wells.

390   The one step ahead simulated groundwater level in the training and testing, and

391 prediction stages by the two models are shown in Fig. 7. For both models, the simulated

392 values completely capture the variation of groundwater levels in monitoring wells with

393 overlapped plot. The R^2 and RMSE values of simulation results are listed in Table 3. In

394 the prediction stage, the values of RMSE are 0.0019 and 0.0166 for BH01 and BH05,

395 and the values of R^2 are larger than 0.999 in the prediction for the TCN-based model.

396 For the LSTM-based model, the RMSE values are 0.0074 and 0.0588, and the R^2 values

397 are 0.9957 and 0.9980. These metrics indicate that both models can "remember" the

398 historical records and produce true observations. The simulation accuracy of TCN-

399 based models is slightly higher than the LSTM-based models. In addition, the running

400 time of the TCN-based model is 2.6 minutes, which is faster than that of the TCN-based

401 model.
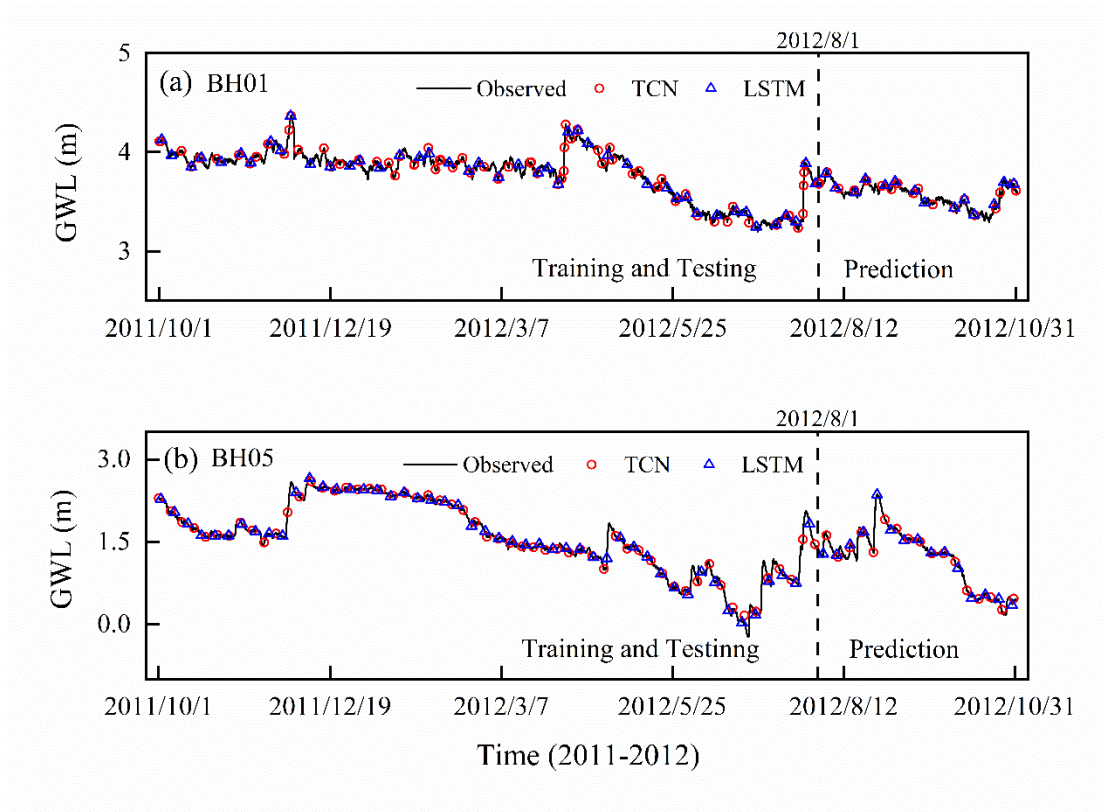
402

403 Figure 7. The simulation results of groundwater level of monitoring wells BH01 and

404 BH05 by TCN-based model. The black dash line divides the data into two groups: the

405 training and testing dataset, and the prediction dataset.

406

407 Table 3. The model results for groundwater level in the training and testing and

408 prediction stage

Well	Model	Training and Testing			Prediction		
		MAE	RMSE	R²	MAE	RMSE	R²
BH01	TCN	0.0017	0.0068	0.9992	0.0009	0.0019	0.9997
	LSTM	0.0053	0.0077	0.9990	0.0050	0.0074	0.9957
BH05	TCN	0.0070	0.0279	0.9981	0.0061	0.0166	0.9990
	LSTM	0.0082	0.0116	0.9997	0.0168	0.0558	0.9980

409

410 **4.4 Long term leading time prediction**

411 The TCN- and LSTM-based models were further adjusted to predict the

412 groundwater levels over three months ahead with different leading period. Prediction

413 results with 1-day, 3-, 7-, and 15-days leading time with TCN- and LSTM-based models

414 are illustrated in Fig. 8 and Fig. 9 for wells BH01 and BH05, respectively. The results

415 show that the predicted groundwater values have the same change trend as the actual

416 groundwater level in monitoring wells. Both of the models are able to capture the

417 variation trend of groundwater levels with longer leading period more than one time

418 step in the two monitoring wells.
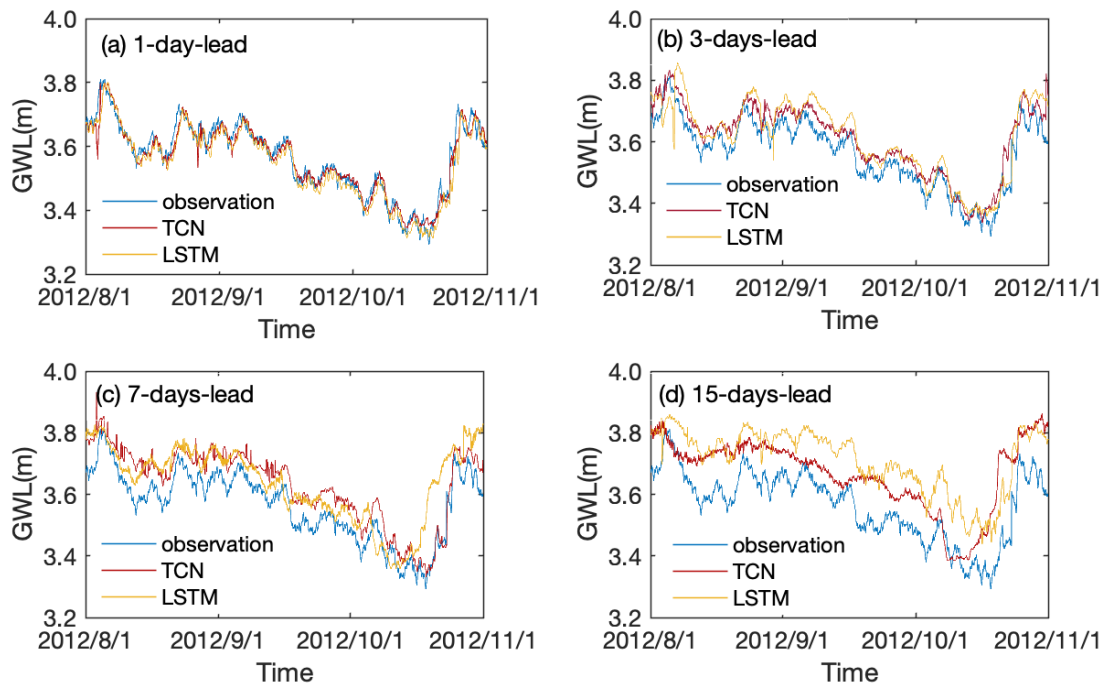
419

420 Figure 8. The observed and predicted values of the groundwater level with TCN- and

421 LSTM-based models for 1-day, 3-, 7- and 15-days lead period in monitoring well BH01.

422
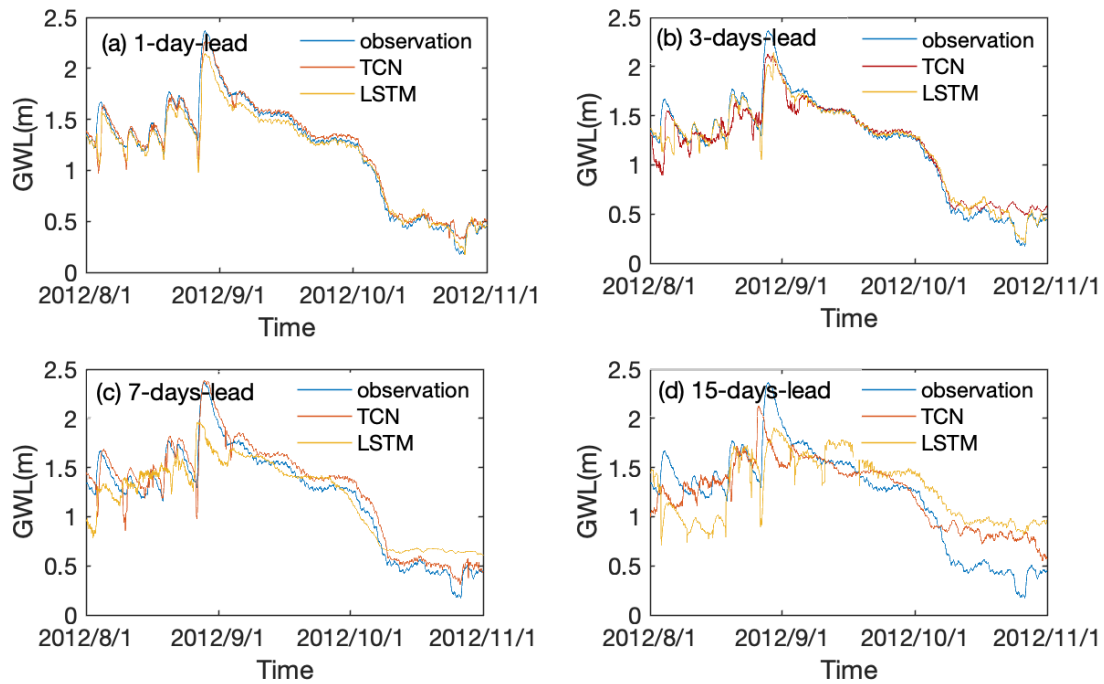
Figure 9. The observed and predicted values of the groundwater level with TCN- and LSTM-based models for 1-day, 3-, 7- and 15-days leading period in monitoring well BH05.

To quantitatively compare the prediction accuracy of the proposed TCN- and LSTM-based models, the results of two evaluation metrics with the model running time are summarized in Table 4. It can be learned that the R^2 value of TCN-based models decreased from 0.9386 to -0.1407 for well BH01 and from 0.9670 to 0.7271 for well BH05. Correspondingly, an increase of RMSE values from 0.028 to 0.1209 and 0.0934 to 0.206 are observed for BH01 and BH05, separately. A similar variation pattern is recognized for LSTM-based model with smaller R^2 and higher RMSE than that of the TCN-based model. Notably, the running time of advance prediction is much longer than that of single step prediction. Meanwhile, with the increasing of leading period, the time had been raised nonlinearly. Further, in this process, the TCN-based model cost longer time than that of LSTM-based model.

438

Table 4. The model results for groundwater level in the long term prediction

| Well | Model | Prediction | | Mins | Model | Prediction | | Mins |
		RMSE	R^2			RMSE	R^2	
BH01	TCN-1	0.0280	0.9386	5.38	LSTM-1	0.0349	0.9047	3.76
	TCN-3	0.0550	0.7638	16.1	LSTM-3	0.0640	0.6802	11.01
	TCN-7	0.0741	0.5713	34.3	LSTM-7	0.0956	0.2874	26.27
	TCN-15	0.1209	-0.1407	94.95	LSTM-15	0.1486	-0.7227	85.13
BH05	TCN-1	0.0934	0.9670	5.19	LSTM-1	0.1012	0.9613	3.78
	TCN-3	0.1375	0.9285	16.18	LSTM-3	0.1086	0.9554	11.4
	TCN-7	0.1084	0.9296	35.44	LSTM-7	0.2050	0.8406	26.2
	TCN-15	0.2060	0.7271	80.46	LSTM-15	0.3515	0.5330	73.45

439

440   The performance of the two networks was further evaluated with Taylor diagrams

441 by taking different criteria aspects which including standard deviation (SD), correlation

442 coefficient (COR), root mean square deviation (RMSD) into account (Taylor, 2001).

443 The comparisons of TCN- and LSTM-based model are shown in Fig. 10. As the metrics

444 distributed away from the reference point (Ref), the deviation of prediction from

445 observation is generally increased with extending of leading period. Taken well BH05

446 for example, the prediction with 1-day (24 hours prediction window) in advance are the

447 highest in agreement with the actual situation in the two models. The 1-day leading

448 prediction results have the lowest RMSD values and highest R^2 values for both models.

449 The prediction precision gradually decreases with the extending of leading time to 3-

450 days, 7-days and 15-days. For well BH01, an out of trending point is observed. The 15-

451 days prediction results of LSTM-based model is closer to the Ref point compared with

452 the TCN-based model. The reason is that the simulation data is highly correlated with

453 observations as shown in Fig.8.

454
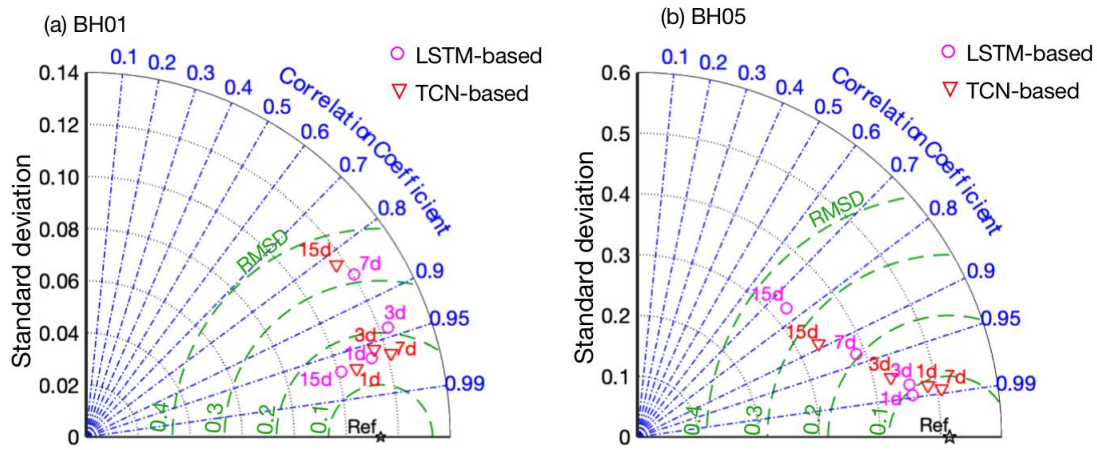
Figure 10. Taylor diagrams with statistical (SD, COR,RMSD) comparison results of

the TCN-based and LSTM-based models for well (a) BH01 (b) BH05.

Overall, the TCN- and LSTM-based models both have strong prediction ability in

long term hydrological time series data. Both models are able to provide accurate

predictions once they are trained. The simulation accuracy of the TCN-based model is

slightly better than that of the LSTM-based model in the three months prediction but

the difference is not significant with p>0.05 in t-test. The causal dilated convolutions

used by TCNs are proved to be good at capturing long-term dependencies of time series

data. Meanwhile, the model precision decreases and the running time increases with

raising leading period. The processing speed of parallel convolution TCN-based models

for long input sequences is slower than that of recurrent networks. This seems to be a

shortage in real-time monitoring and early warning. A leading period shorter than 7

days is recommended to ensure both of the accuracy and efficiency of the models in

real-time monitoring and early warning.

4.5 Influence of training set percentage

The data-driven methods are supported by data; however, how much data is needed

471 to build an effective model is still a challenging problem (Reichstein et al., 2019). This

472 is because specific problems depend on application cases, data features, and model

473 features (Wunsch et al., 2021). Here we discuss the effect of training set percentage on

474 the TCN- and LSTM-based models. In our study, the data is the hourly-monitored data

475 from 2011 to 2012. From 2011, we set 20%, 30% to 90% training sets in turn, so as to

476 gradually expand the length of training set.

477   Fig. 11 shows the effect of increased percentage of training set on the performance

478 of the model. All experiments were repeated five times, and the average values of each

479 index were compared. It can be seen that the performance of the TCN-based model

480 improved with the increase of the percentage of training set. When the training set

481 reached 80%, the performance was relatively optimal, and then the performance began

482 to deteriorate with the increase of the percentage of training set. At the same time, it

483 can be seen that the performance of the LSTM-based model tends to be stable when the

484 training set reaches 70%, and then decreases slightly with the increase of training set.

485 Therefore, a training set evaluation is recommended before the training and testing. We

486 should carefully evaluate and shorten the training data set as much as possible when

487 necessary. Finally, we set 80% of the training set length to simulate the coastal aquifer

488 time-series data.
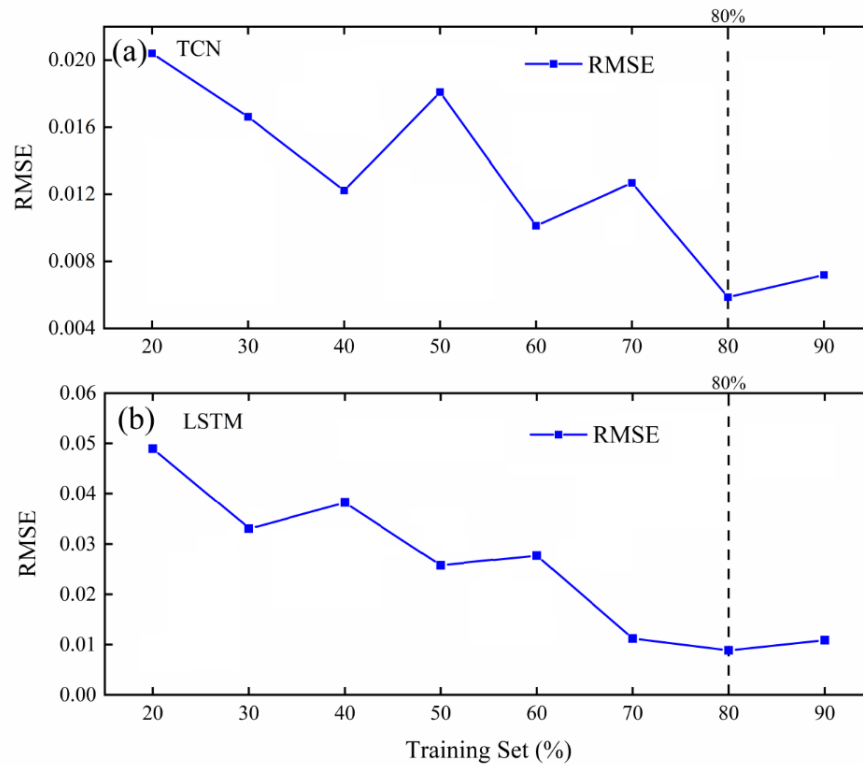
490 Figure 11. Influence of training set percentage on the performance of the model for (a)

491 BH01 and (b) BH05.

492 **5 Conclusions**

493 The TCN- and LSTM-based deep learning models were proposed in this paper to

494 predict groundwater levels in a coastal aquifers. Hyper-parameter searches was first

495 conducted to obtain good architecture configurations. The results indicated that a deeper,

496 broader model does not necessarily guarantee better predictions. The optimal

497 configurations then were adopted for the networks of all monitoring data. Both of the

498 TCN- and LSTM- based model well captured the fluctuation of groundwater levels and

499 achieved satisfactory performance on the prediction. Meanwhile, a decreasing precision

500 is revealed when the leading time increases in advance prediction. In view of accuracy,

501 the TCN-based model outperforms the LSTM-based model but less efficiency in long-

term simulation. Thus, both models can bu used as promising method for time-series

prediction of hydrogeological data especially when the regional data is difficult to

collect in a complex system.

~~To validate the newly developed TCN-based model, its performance is compared~~

~~with the LSTM-based recurrent networks. The TCN-based model outperforms the~~

~~LSTM-based model in view of both accuracy and efficiency. Meanwhile, three months~~

~~ahead predictions were conducted with different leading periods. A decreasing precision~~

~~is revealed when the leading time increases. In particular, once TCN was trained, due~~

~~to the use of parallel convolution to process the input sequence, its prediction speed is~~

~~significantly faster than recurrent networks. In summary, our research shows that TCN~~

~~is a very powerful alternative to the LSTM network. It can provide accurate predictions~~

~~and is suitable for more complex real-time applications because of its high efficiency.~~

Acknowledgements

This work was jointly supported by National Natural Science Foundation of

China (No: 41702244), the Program for Jilin University (JLU) Science and Technology

Innovative Research Team (No. 2019TD-35).

Code availability

The pieces of code that were used for all analyses are available from the authors

upon request.

Data availability

The data sets that have been analyzed in this paper are available from the

authors upon request.

Author contribution

XZ drafted the manuscript and revised the manuscript. GC designed the experiments and collected all the data. DF developed the model code and performed the simulations. ZD was responsible for the project design, oversaw the analysis, and conducted manuscript revision as the project leader and the senior scientist.

Competing interests

The authors declare that they have no conflict of interest.

Reference

Abdalla, O. A. and Al-Rawahi, A. S.: Groundwater recharge dams in arid areas as tools for aquifer replenishment and mitigating seawater intrusion: example of AlKhod, Oman, Environ. Earth Sci., 69, 1951-1962, 2013.

Adam, D. K. J. B.: A method for stochastic optimization in: 3rd International Conference on Learning Representations, 2015.

Afaq, S. and Rao, S.: Significance of epochs on training a neural network, International Journal of Scientific & Technology Research, 9, 485-488, 2020.

Baena-Ruiz, L., Pulido-Velazquez, D., Collados-Lara, A.-J., Renau-Pruñonosa, A., and Morell, I.: Global assessment of seawater intrusion problems (status and vulnerability), Water Resour. Manag., 32, 2681-2700, 2018.

Bai, S., Kolter, J. Z., and Koltun, V.: An empirical evaluation of generic convolutional and recurrent networks for sequence modeling, arXiv preprint arXiv:1803.01271, 2018.

Barlow, P. M. and Reichard, E. G.: Saltwater intrusion in coastal regions of North America, Hydrogeol. J., 18, 247-260, 2010.

Batelaan, O., De Smedt, F., and Triest, L.: Regional groundwater discharge: phreatophyte mapping, groundwater modelling and impact analysis of land-use change, J. Hydrol., 275, 86-108, 2003.

Bengio, Y., Simard, P., and Frasconi, P.: Learning long-term dependencies with gradient descent is difficult, IEEE Trans. Neural Netw., 5, 157-166, 1994.

Borovykh, A., Bohte, S., and Oosterlee, C. W.: Dilated convolutional neural networks for time series forecasting, J. Comput. Financ., 2018.

Cannas, B., Fanni, A., See, L., and Sias, G.: Data preprocessing for river flow forecasting using neural networks: wavelet transforms and data partitioning, Phys. Chem. Earth, 31, 1164-1171, 2006.

Cao, Y., Ding, Y., Jia, M., and Tian, R.: A novel temporal convolutional network with residual self-attention mechanism for remaining useful life prediction of rolling bearings, Reliab. Eng. Syst. Saf., 215, 107813, 2021.

Chen, Y., Kang, Y., Chen, Y., and Wang, Z.: Probabilistic forecasting with temporal convolutional neural network, Neurocomputing, 399, 491-501, 2020.

Coulibaly, P., Anctil, F., Aravena, R., and Bobée, B.: Artificial neural network modeling of water table depth fluctuations, Water Resour. Res., 37, 885-896, 2001.

Dai, Z. and Samper, J.: Inverse modeling of water flow and multicomponent reactive transport in coastal aquifer systems, J. Hydrol., 327, 447-461, 2006.

Dai, Z., Xu, L., Xiao, T., McPherson, B., Zhang, X., Zheng, L., Dong, S., Yang, Z., Soltanian, M. R., and Yang, C.: Reactive chemical transport simulations of geologic carbon sequestration: Methods and applications, Earth-Sci. Rev., 208, 103265, 2020.

Dubey, A. K., Kumar, A., García-Díaz, V., Sharma, A. K., and Kanhaiya, K.: Study and analysis of SARIMA and LSTM in forecasting time series data, Sustain. Energy Technol. Assess., 47, 101474, 2021.

Ergen, T. and Kozat, S. S.: Efficient online learning algorithms based on LSTM neural networks, IEEE Trans. Neural Netw. Learn. Syst., 29, 3772-3783, 2017.

Feng, N., Geng, X., and Qin, L.: Study on MRI medical image segmentation technology based on CNN-CRF model, IEEE Access, 8, 60505-60514, 2020.

Fischer, T. and Krauss, C.: Deep learning with long short-term memory networks for financial market predictions, Eur. J. Oper. Res., 270, 654-669, 2018.

Gan, Z., Li, C., Zhou, J., and Tang, G.: Temporal convolutional networks interval prediction model for wind speed forecasting, Electr. Power Syst. Res., 191, 106865, 2021.

Garza-Díaz, L. E., DeVincentis, A. J., Sandoval-Solis, S., Azizipour, M., Ortiz-Partida, J. P., Mahlknecht, J., Cahn, M., Medellín-Azuara, J., Zaccaria, D., and Kisekka, I.: Land-use optimization for sustainable agricultural water management in Pajaro Valley, California, J. Water Resour. Plan. Manage.-ASCE, 145, 05019018-05019018, 2019.

Gorgij, A. D., Kisi, O., and Moghaddam, A. A.: Groundwater budget forecasting, using hybrid wavelet-ANN-GP modelling: a case study of Azarshahr Plain, East Azerbaijan, Iran, Hydrol. Res., 48, 455-467, 2017.

Han, D., Kohfahl, C., Song, X., Xiao, G., and Yang, J.: Geochemical and isotopic evidence for palaeo-seawater intrusion into the south coast aquifer of Laizhou Bay, China, Appl. Geochem., 26, 863-883, 2011.

Han, D., Song, X., Currell, M. J., Yang, J., and Xiao, G.: Chemical and isotopic constraints on evolution of groundwater salinization in the coastal plain aquifer of Laizhou Bay, China, J. Hydrol., 508, 12-27, 2014.

He, K., Zhang, X., Ren, S., and Sun, J.: Deep residual learning for image recognition, Proc. IEEE, 770-778,

Huang, F.-K., Chuang, M.-H., Wang, G. S., and Yeh, H.-D.: Tide-induced groundwater level fluctuation in a U-shaped coastal aquifer, J. Hydrol., 530, 291-305, 2015.

Jiang, Y., Zhao, M., Zhao, W., Qin, H., Qi, H., Wang, K., and Wang, C.: Prediction of sea temperature using temporal convolutional network and LSTM-GRU network, Complex Engineering Systems, 1, -, 2021.

Ketabchi, H. and Ataie-Ashtiani, B.: Evolutionary algorithms for the optimal management of coastal groundwater: A comparative study toward future challenges,

J. Hydrol., 520, 193-213, 2015.

Kratzert, F., Herrnegger, M., Klotz, D., Hochreiter, S., and Klambauer, G.: NeuralHydrology–interpreting LSTMs in hydrology, in: Explainable AI: Interpreting, explaining and visualizing deep learning, Springer, 347-362, 2019.

Kreyenberg, P. J., Bauser, H. H., and Roth, K.: Velocity field estimation on density-driven solute transport with a convolutional neural network, Water Resour. Res., 55, 7275-7293, 2019.

Lara-Benítez, P., Carranza-García, M., Luna-Romera, J. M., and Riquelme, J. C.: Temporal convolutional networks applied to energy-related time series forecasting, applied sciences, 10, 2322, 2020.

Lea, C., Vidal, R., Reiter, A., and Hager, G. D.: Temporal convolutional networks: A unified approach to action segmentation, European conference on computer vision, 47-54,

Lea, C., Flynn, M. D., Vidal, R., Reiter, A., and Hager, G. D.: Temporal convolutional networks for action segmentation and detection, Proc. IEEE, 156-165,

LeCun, Y., Bottou, L., Bengio, Y., and Haffner, P.: Gradient-based learning applied to document recognition, Proc. IEEE, 86, 2278-2324, 1998.

Li, H., Jiao, J. J., Luk, M., and Cheung, K.: Tide-induced groundwater level fluctuation in coastal aquifers bounded by L-shaped coastlines, Water Resour. Res., 38, 6-1-6-8, 2002.

Long, J., Shelhamer, E., and Darrell, T.: Fully convolutional networks for semantic segmentation, Proc. IEEE, 3431-3440,

Lu, C., Werner, A. D., and Simmons, C. T.: Threats to coastal aquifers, Nature Climate Change, 3, 605-605, 2013.

Lu, C., Cao, H., Ma, J., Shi, W., Rathore, S. S., Wu, J., and Luo, J.: A proof-of-concept study of using a less permeable slice along the shoreline to increase fresh groundwater storage of oceanic islands: Analytical and experimental validation, Water Resour. Res., 55, 6450-6463, 2019.

Maier, H. R. and Dandy, G. C.: Neural networks for the prediction and forecasting of water resources variables: a review of modelling issues and applications, Environ. Modell. Softw., 15, 101-124, 2000.

Mehr, A. D. and Nourani, V.: A Pareto-optimal moving average-multigene genetic programming model for rainfall-runoff modelling, Environ. Modell. Softw., 92, 239-251, 2017.

Mei, Y., Tan, G., and Liu, Z.: An improved brain-inspired emotional learning algorithm for fast classification, Algorithms, 10, 70, 2017.

Nair, V. and Hinton, G. E.: Rectified linear units improve restricted boltzmann machines, Icml,

Park, Y., Lee, J.-Y., Kim, J.-H., and Song, S.-H.: National scale evaluation of groundwater chemistry in Korea coastal aquifers: evidences of seawater intrusion, Environ. Earth Sci., 66, 707-718, 2012.

Pascanu, R., Mikolov, T., and Bengio, Y.: On the difficulty of training recurrent neural networks, International conference on machine learning, 1310-1318, 2013.

Pratheepa, V., Ramesh, S., Sukumaran, N., and Murugesan, A.: Identification of the

648   sources for groundwater salinization in the coastal aquifers of Southern Tamil Nadu,
649   India, Environ. Earth Sci., 74, 2819-2829, 2015.

650   Reichstein, M., Camps-Valls, G., Stevens, B., Jung, M., Denzler, J., and Carvalhais, N.:
651   Deep learning and process understanding for data-driven Earth system science,
652   Nature, 566, 195-204, 2019.

653   Rumelhart, D. E., Hinton, G. E., and Williams, R. J.: Learning representations by back-
654   propagating errors, Nature, 323, 533-536, 1986.

655   Sahoo, S., Russo, T., Elliott, J., and Foster, I.: Machine learning algorithms for
656   modeling groundwater level changes in agricultural regions of the US, Water Resour.
657   Res., 53, 3878-3895, 2017.

658   Salimans, T. and Kingma, D. P.: Weight normalization: A simple reparameterization to
659   accelerate training of deep neural networks, Advances in neural information
660   processing systems, 29, 2016.

661   Senthil Kumar, A., Sudheer, K., Jain, S., and Agarwal, P.: Rainfall-runoff modelling
662   using artificial neural networks: comparison of network types, Hydrological
663   Processes: An International Journal, 19, 1277-1291, 2005.

664   Seo, Y., Kim, S., Kisi, O., and Singh, V. P.: Daily water level forecasting using wavelet
665   decomposition and artificial intelligence techniques, J. Hydrol., 520, 224-243, 2015.

666   Solgi, R., Loáiciga, H. A., and Kram, M.: Long short-term memory neural network
667   (LSTM-NN) for aquifer level time series forecasting using in-situ piezometric
668   observations, J. Hydrol., 601, 126800, 2021.

669   Srivastava, N., Hinton, G., Krizhevsky, A., Sutskever, I., and Salakhutdinov, R.:
670   Dropout: a simple way to prevent neural networks from overfitting, J. Mach. Learn.
671   Res., 15, 1929-1958, 2014.

672   Taylor, K. E.: Summarizing multiple aspects of model performance in a single diagram,
673   J. Geophys. Res.-Atmos., 106, 7183-7192, 2001.

674   Torres, J. F., Troncoso, A., Koprinska, I., Wang, Z., and Martínez-Álvarez, F.: Deep
675   learning for big data time series forecasting applied to solar power, The 13th
676   International Conference on Soft Computing Models in Industrial and
677   Environmental Applications, 123-133, 2018.

678   Wan, R., Mei, S., Wang, J., Liu, M., and Yang, F.: Multivariate temporal convolutional
679   network: A deep neural networks approach for multivariate time series forecasting,
680   Electronics, 8, 876, 2019.

681   Wunsch, A., Liesch, T., and Broda, S.: Groundwater level forecasting with artificial
682   neural networks: a comparison of long short-term memory (LSTM), convolutional
683   neural networks (CNNs), and non-linear autoregressive networks with exogenous
684   input (NARX), Hydrol. Earth Syst. Sci., 25, 1671-1687, 2021.

685   Xu, Z. and Hu, B. X.: Development of a discrete-continuum VDFST-CFP numerical
686   model for simulating seawater intrusion to a coastal karst aquifer with a conduit
687   system, Water Resour. Res., 53, 688-711, 2017.

688   Xue, Y., Wu, J., Ye, S., and Zhang, Y.: Hydrogeological and hydrogeochemical studies
689   for salt water intrusion on the south coast of Laizhou Bay, China, Groundwater, 38,
690   38-45, 2000.

691   Yan, J., Mu, L., Wang, L., Ranjan, R., and Zomaya, A. Y.: Temporal convolutional

networks for the advance prediction of ENSO, Sci Rep, 10, 1-15, 2020.

Zeng, X., Wu, J., Wang, D., and Zhu, X.: Assessing the pollution risk of a groundwater source field at western Laizhou Bay under seawater intrusion, Environ. Res., 148, 586-594, 2016.

Zhan, C., Dai, Z., Soltanian, M. R., and Zhang, X.: Stage-wise stochastic deep learning inversion framework for subsurface sedimentary structure identification, Geophys. Res. Lett., 49, e2021GL095823, 2022.

Zhang, D., Lin, J., Peng, Q., Wang, D., Yang, T., Sorooshian, S., Liu, X., and Zhuang, J.: Modeling and simulating of reservoir operation using the artificial neural network, support vector regression, deep learning algorithm, J. Hydrol., 565, 720-736, 2018a.

Zhang, J., Zhu, Y., Zhang, X., Ye, M., and Yang, J.: Developing a Long Short-Term Memory (LSTM) based model for predicting water table depth in agricultural areas, J. Hydrol., 561, 918-929, 2018b.

Zhang, J., Zhang, X., Niu, J., Hu, B. X., Soltanian, M. R., Qiu, H., and Yang, L.: Prediction of groundwater level in seashore reclaimed land using wavelet and artificial neural network-based hybrid model, J. Hydrol., 577, 123948, 2019.

Zhang, X., Miao, J., Hu, B. X., Liu, H., Zhang, H., and Ma, Z.: Hydrogeochemical characterization and groundwater quality assessment in intruded coastal brine aquifers (Laizhou Bay, China), Environ. Sci. Pollut. Res., 24, 21073-21090, 2017.

Zhang, X., Dong, F., Dai, H., Hu, B. X., Qin, G., Li, D., Lv, X., Dai, Z., and Soltanian, M. R.: Influence of lunar semidiurnal tides on groundwater dynamics in estuarine aquifers, Hydrogeol. J., 28, 1419-1429, 2020.